

Article

Not peer-reviewed version

Aluminum-Based Plasmonic Photodetector for Sensing Applications

Yurii Lyaschuk , Ivan Indutnyi , Viktor Myn'ko , Volodymyr Romanyuk , Iryna Mamontova , Roman Redko , [Mykhailo Dusheyko](#) , Yelizaveta Savchuk , Vasyi Tochkovyi , Oleksandr Shtykalo , Daria Kuznetsova , [Sergii Mamykin](#) *

Posted Date: 25 April 2024

doi: 10.20944/preprints202404.1645.v1

Keywords: plasmon-polariton photodetectors; surface plasmon resonance; diffraction gratings; optochemical sensors



Preprints.org is a free multidiscipline platform providing preprint service that is dedicated to making early versions of research outputs permanently available and citable. Preprints posted at Preprints.org appear in Web of Science, Crossref, Google Scholar, Scilit, Europe PMC.

Copyright: This is an open access article distributed under the Creative Commons Attribution License which permits unrestricted use, distribution, and reproduction in any medium, provided the original work is properly cited.

Article

Aluminum-Based Plasmonic Photodetector for Sensing Applications

Yurii Lyashchuk¹, Ivan Indutnyi¹, Viktor Myn'ko¹, Volodymyr Romanyuk¹, Iryna Mamontova¹, Roman Redko^{1,2}, Mykhailo Dusheyko¹, Yelizaveta Savchuk¹, Vasyl Tochkovyi¹, Oleksandr Shtykalo¹, Daria Kuznetsova¹ and Sergii Mamykin^{1,3,*}

¹ V.E. Lashkaryov Institute of Semiconductor Physics, National Academy of Sciences of Ukraine, 41, Nauky pr., 03028, Kyiv, Ukraine; yulashchuk@gmail.com; (Yu.L.); indutnyy@isp.kiev.ua (I.I.); mynkoviktor@gmail.com (V.M.); romanyuk@isp.kiev.ua (V.R.); mirina@isp.kiev.ua (I.M.); redko.rom@gmail.com (R.R.); mgd61@ukr.net (M.D.); liza.synelnyk@gmail.com (Ye.S.); to4ckowy@gmail.com (V.T.); astrosasha013@gmail.com (O.Sh.); dasha.kuznetsova.j@gmail.com (D.K.); mamykin@isp.kiev.ua (S.M.);

² State University of Information and Communication Technologies, 7, Solomenska st., 03680 Kyiv, Ukraine

³ Physics Department, National Taras Shevchenko Kyiv University, 4, Akademik Glushkov prosp., 03127 Kyiv, Ukraine

* Correspondence: mamykin@isp.kiev.ua

Abstract: Plasmonic sensors have great potential for widespread usage, but the prohibitive cost of noble metals restrains the wider adoption of this technology. The aim of our study is to develop a cost-effective Al-based alternative to plasmonic detectors commonly based on noble metals. We considered a structure that consists of a Si p-n junction with an overlying grating-relief aluminum layer. The investigation of the infrared plasmonic resonance dependency on the structure geometric parameters and optimization of the fabrication process allowed us to determine optimal parameters for photodetection enhancement. The resonance photoresponse of optimized aluminum-based plasmon-polariton photodetector was significantly improved and became comparable to noble metal-based analogs. Our results can be used for the creation of cost-effective high-sensitivity plasmonic sensors.

Keywords: plasmon-polariton photodetectors; surface plasmon resonance; diffraction gratings; optochemical sensors

1. Introduction

Surface plasmon polaritons (SPP) are electromagnetic surface waves propagating along the boundary between metal and dielectric or semiconductor with the maximum field located at this interface and decaying exponentially in both media [1]. Being a non-radiative mode, such a surface wave requires matching of its wave vector with the wave vector of incident light, which in most cases is accomplished using a coupling prism [2–4] or a diffraction grating [5–8]. Under optimal conditions, complete transformation of light energy into the energy of surface plasmon polaritons is achieved, accompanied by a local increase in the intensity of the electromagnetic field at the interface with the metal plasmon-carrying film. Such spatial localization of the electromagnetic field at an energy of incident photons greater than the band gap of the semiconductor contributes to an increase in the generation of electron-hole pairs in it near the contact with the metal and a corresponding increase in the photocurrent in the presence of a built-in electric field separating charge carriers. At energies lower than the band gap, excitation of hot electrons in the metal-plasmon-carrying film with subsequent ballistic transport to the semiconductor region with built-in electric field is possible [9–12]. Thus, the spectral sensitivity range of such photodetectors can extend beyond the band-to-band generation region by expanding into the red spectral region. Based on this phenomenon, the design

of a so-called plasmon-polariton photodetector (PPPD) was proposed [9,13,14]. To excite SPPs in such detectors, a periodically textured semiconductor surface (diffraction grating) with a thin layer of plasmonic metal deposited on it is used. GaAs, Si, InP were proposed as semiconductors, and films of noble metals Au and Ag as well as Al films were used mainly as plasmon-carrying metals [15,16]. The application area of such photodetectors is quite wide – they are used in sensing, photovoltaics, telecommunications, etc. [15–19]. A basic principle underlying the device operation is the resonant enhancement of the short-circuit photocurrent generated under surface plasmon resonance (SPR) conditions in a Schottky junction at the metal-semiconductor contact [9,20]. However, the presence of a corrugated interface at the Schottky junction contributes to enhanced carrier recombination and scattering, leading to the attenuation of the useful signal. In this regard, PPPD designs with a flat metal-semiconductor interface have been proposed, with the grating relief formed on the outer side of the plasmon-carrying metallic film [21].

For PPPDs based on n-type doped silicon, a scheme using a shallow p-n junction has been proposed, where the distance from the plasmon-carrying metal layer to the p-n junction is about 100 nm [22]. This approach eliminates the need to form a high Schottky barrier at the metal-semiconductor interface, which is not always possible in Au/Si or Al/Si pairs. In this case, the separation of photo-carriers occurs in the p-n junction region, remote from the metal/Si interface, which is characterized by a high surface recombination rate. The influence of deep levels formed by Au in Si on the increase in recombination is also reduced. Moreover, the metal/Si interface can remain flat, simplifying the manufacturing process.

Most studies on PPPDs have been carried out on structures using noble metals, mainly gold. Gold has slightly worse plasmonic characteristics (in particular, the ratio of the real and imaginary parts of the dielectric constant) than silver, but it is much more resistant to degradation during operation. It was shown in [19,23] that cheaper aluminum has plasmonic characteristics even better than gold in a significant spectral range, especially in the blue and ultraviolet parts of the spectrum. At the same time, aluminum films are naturally oxidized in air at room temperature to form a relatively stable Al_2O_3 dielectric layer, which subsequently protects the plasmon-carrying metal layer from degradation. The performance of PPPDs based on aluminum may be optimized for specific applications by choosing the optimal grating geometric characteristics.

In this work, the parameters of PPPDs based on silicon p-n junctions and aluminum as the plasmon-carrying metal have been optimized. An optochemical sensor has been chosen as a specific application device, where PPPD is used as an optical sensor. Using the RCWA method [24,25], theoretical simulations of the electromagnetic field intensity distribution in the proposed PPPD structure have been carried out, and optimal characteristics of the plasmon-carrying layer grating have been selected. Experimental samples of PPPDs with optimal aluminum gratings have been fabricated, their characteristics have been investigated, and it has been shown that the polarization sensitivity of these samples is comparable to the results obtained on PPPDs with gold films. The proposed PPPD design includes only Al, Cr, Si, Ti significantly reducing production costs.

2. Materials and Methods

2.1. Fabrication of PPPDs on Si Substrates

For the fabrication of PPPDs, a pre-made p-n junction on n-Si (111) with a burial depth of 100 nm and formed ohmic rear contacts with Ti/Ni 25/250 nm were utilized. The necessary periodic relief structures (gratings) on the silicon surface were created using the method of interference lithography with thermally deposited in vacuum chalcogenide photoresist [21]. A particular feature of this technology, compared to the standard one where the grating is etched into the semiconductor, is the profiling exclusively of the metallic plasmon-carrying Al film. This maintains a flat metal/semiconductor interface with low recombination of photo-generated carriers. Such a PPPD has a simpler construction and good resonant properties [21].

A schematic representation of the step-by-step (1-7) process of fabricating Al gratings on the Si surface is shown in Figure 1. Before installation into the vacuum chamber, the working side of the Si wafer was cleaned in ethyl alcohol and a 5% aqueous solution of HF, followed by rinsing with

distilled water and drying with compressed air (Figure 1, 1). The subsequent steps involved sequential vacuum thermal deposition of an adhesive Cr layer with a mass thickness of ~ 3 nm and an Al layer of optimal thickness onto the Si surface (Figure 1, 2). This thickness will determine the depth of modulation of the surface relief, D . After cooling the wafer to room temperature, a layer of photoresist $As_{40}S_{40}Se_{20}$ with a thickness of ~ 150 nm was deposited on the Al surface (Figure 1, 3). The photoresist was exposed in the interference zone of two coherent laser beams emitted by a helium-cadmium laser (wavelength $\lambda = 441.6$ nm). The spatial period of light intensity distribution in the interference zone depended on the convergence angle of the beams and determined the grating period, a . After exposure, selective etching of the photoresist was performed to form a mask that allows access of the etchant to the open areas of the Al layer (Figure 1, 4).

The etchant used for the photoresist $As_{40}S_{40}Se_{20}$ contained ethylenediamine ($C_2H_8N_2$) as an active substance and dimethyl sulfoxide (C_2H_6OS) as a solvent, in a ratio of $\sim 1:9$. At the optimal etchant temperature ($20\text{--}25^\circ\text{C}$), the etching process took about 3 minutes. After creating the relief lithographic mask, the Al layer in the mask openings was removed using an etchant based on orthophosphoric (H_3PO_4), acetic (H_3COOH) acids, and distilled water in a ratio of 6:2:2 (Figure 1, 5). The final steps of forming the relief structure of the PPPD involved removing the lithographic mask (Figure 1, 6) and vacuum thermal deposition of an additional Al layer of thickness d onto the obtained relief (Figure 1, 7). The aluminum grating on the silicon wafer surface provided excitation of SPR and also served as the upper electrical contact.

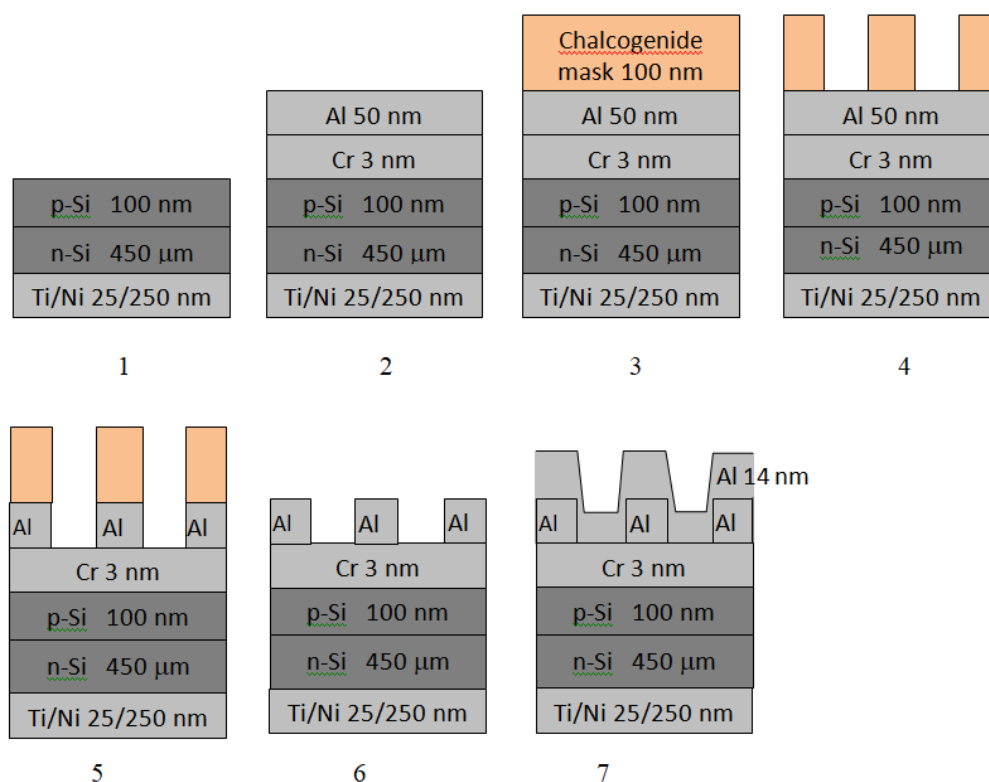


Figure 1. Key stages of manufacturing a PPPD using aluminum as the plasmon-carrying metal.

2.2. Morphological Characterization

The surfaces of the gratings were morphologically characterized using a Dimension 3000 Scanning Probe atomic force microscope (Digital Instruments Inc., Tonawanda, NY, USA) in tapping mode. Figure 2 shows a cross-section of the surface microrelief of several manufactured PPPDs with a plane perpendicular to the Al grating grooves.

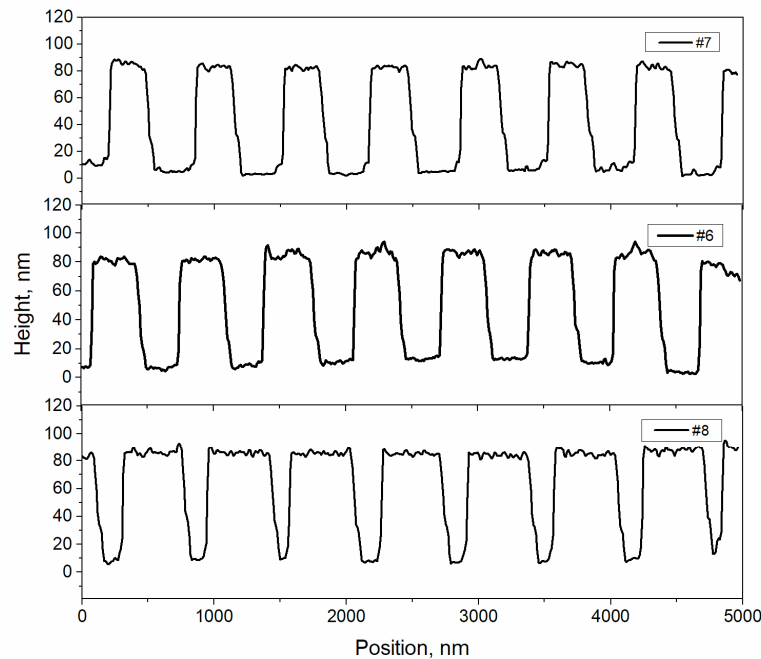


Figure 2. AFM cross-sections of the Al gratings on the surface of the Si wafer.

It can be observed that the cross-sectional shape of the grating grooves is close to a trapezoid with varying filling factor (i.e., the ratio of the groove width to the grating period). The parameters of the trapezoid and filling factor are determined by the parameters of the interference lithography process - exposure time, etching time, characteristics of the resist and selective etchant. By varying these parameters, the characteristics of the grating can be optimized in accordance with the results of numerical modeling, which are presented in the following section of this article.

2.3. Optical Characterizations

Optical constants (refractive index, n , and extinction coefficient, k) of thin aluminum films deposited on substrates by vacuum thermal evaporation were measured in the spectral range of 250-2100 nm using a SE-2000 (Semilab Ltd.) spectroscopic ellipsometer. Figures 3a,b present the spectral dependencies of the refractive index n and extinction coefficient k for Al films without thermal annealing after sputtering. As seen from the figures, the optical constants of thin films some differs from the literature data, which typically correspond to bulk materials. This deviation between the measured optical constants for thin films and the literature data is primarily due to enhanced electron scattering at film boundaries and spatial confinement effects. It is crucial to consider this phenomenon when modeling the resonant properties of PPPDs to ensure accurate predictions and optimized device performance.

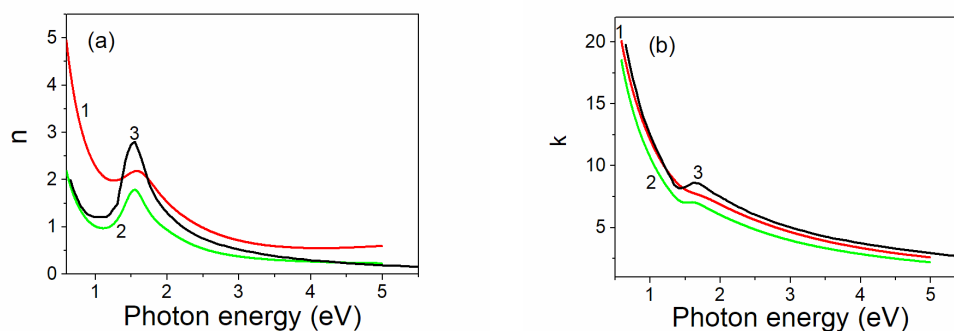


Figure 3. Spectral dependences of (a) refractive index n and (b) extinction coefficient k for Al films of 15 nm (curve1) and 50 nm (2) thicknesses, (3) – literature data [26] for bulk material.

The spectral and angular dependences of the short-circuit photocurrent i_{ph} of manufactured PPPD samples were also studied under illumination with p- and s-polarized light in the wavelength range of 0.4-1.1 μm and incidence angles $\theta = 0 - 70^\circ$. The measuring setup includes a tungsten lamp light source, light chopper, monochromator, polarizer of the Glan prism type, photodetector with an amplifier, rotating sample holder, and controller computer [27].

3. Theoretic Simulation of the Proposed Structure and Parameter Optimization

3.1. Description of the Geometry of the Structure

In order to conduct a rigorous electrodynamic simulation of the PPPD structure, we need to choose an idealized geometric profile for the grating that can be successfully simulated by available numerical methods without significant deviation from the real-world structure profile. A rectangular profile is the most efficient for numerical simulation, but the results of calculations for such a profile are poorly correlated with experimental spectra, presumably because of some deviation from the actual profile. Conversely, different smoothed profiles are far better for describing the actual profile but can undermine calculation stability and require a much larger amount of computation with diminishing returns of accuracy. The trapezoidal profile is the best option for our goals: it allows relatively quick exploration of the parameter space while providing sufficient calculation accuracy. In addition, the groove profiles of aluminum gratings obtained experimentally using interference lithography (Figure 2) are close to trapezoidal. Therefore, Figure 4 provides a schematic sketch of the simulated PPPD structure, highlighting the metallic (Al) grating and the silicon substrate. The grating parameters are chosen to satisfy phase-matching conditions that allow the excitation of SPPs. These resonant modes enhance light absorption within the depletion region of the p-n junction (not shown here), leading to increased generation of electron-hole pairs and resonant photocurrent enhancement.

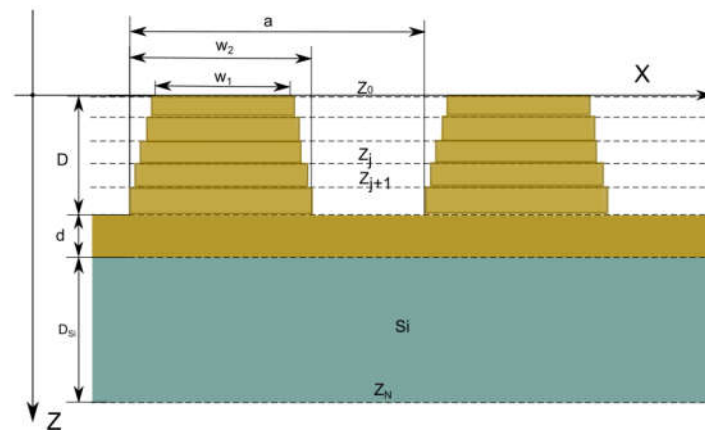


Figure 4. A schematic sketch of the structure, where a is the grating period, w_1 , w_2 , are the base lengths of trapezoidal profile, d is the thickness of intermediate metal layer, D is the depth of grating grooves.

3.2. Parameters Estimation from Dispersion Curves

The grating period can be estimated from the phase-matching conditions for SPP excitation for a given angle of incidence and wavelength. If the simulated PPPD is intended for use in an optochemical sensor, then due to the design of this sensor, the resonant angle of incidence of the laser beam of the most available laser on the market with a wavelength of 808 nm on the grating (the angle corresponding to the excitation of the SPP) should be equal to $\theta_r = 15^\circ$. Taking into account the dispersion relations for SPP plasmons, the phase-matching condition for p-polarized laser radiation, the plane of incidence of which on the grating is perpendicular to its grooves, can be written as follows:

$$\text{Re} [k_{\text{SPP}}] = k_{\text{inc}} + G_m, \quad (1)$$

where k_{SPP} is the SPP wavevector $k_{\text{inc}} = \left(\frac{\sqrt{\varepsilon_d} 2\pi}{\lambda}\right) \sin \theta$ is the surface component of incident light wavevector, ε_d is the dielectric constant of the environment, θ is the angle of incidence, and G_m is the grating vector $G_m = 2\pi m/a$, m - an integer ($m \neq 0$). Using for k_{SPP} the approximation of a flat interface between the metal and the dielectric (valid for gratings with shallow relief): $k_{\text{SPP}} = \left(\frac{2\pi}{\lambda}\right) \sqrt{\varepsilon_m \varepsilon_d / (\varepsilon_m + \varepsilon_d)}$, where ε_m is the dielectric constant of the metal, and $\varepsilon_d = 1$ we can rewrite expression (1):

$$\pm \frac{|m|}{a} = \frac{1}{\lambda} \text{Re} \sqrt{\frac{\varepsilon_m}{\varepsilon_m + 1}} \pm \frac{1}{\lambda} \sin |\theta|, \quad (2)$$

finally, we get an expression for the grating period

$$a = \frac{|m|\lambda}{\text{Re} \sqrt{\frac{\varepsilon_m}{\varepsilon_m + 1}} \pm \sin |\theta|}, \quad (3)$$

For the first-order SPP resonance $|m|=1$, expression (3) gives values $a \approx 1.1 \mu\text{m}$ and $a \approx 0.63 \mu\text{m}$. For the grating with $a = 1.1 \mu\text{m}$, there is an additional (the second) maximum on angle and spectral dependences of the photocurrent, which can be significantly wider than the first one and cause occlusion and blurring of the main maximum. Therefore, it is more convenient to have only one SPP resonance for registering external influences without any interference from the second one. Thus, we choose the grating period $a = 0.63 \mu\text{m}$.

The sensitivity of the PPPD is primarily affected by the number of photons absorbed in the semiconductor (taking into account its intensity distribution). To determine these parameters, we should carry out a full rigorous electrodynamics simulation of the plasmonic structure under consideration.

3.3. Theoretical Methods Description

One of the most suitable methods applicable to modeling such periodic structures is RCWA (Rigorous coupled-wave analysis) [24], sometimes called FMM (Fourier modal method). We implemented an improved formulation of RCWA which uses an inverse factorization rule that improves convergence and speed of calculation for p-polarization [28]. Although this method was developed primarily for the simulation of rectangular gratings, it can be applicable to a variety of periodic profiles. It can be achieved by reducing an arbitrary periodic profile into a set of thin slices each of which can be approximated by a rectangular profile. This method has advantages compared to methods that use discretization in real space, such as finite element methods, or finite difference methods, such as relative simplicity of implementation and low computational resource requirements. This method allows calculation of reflection and transmission coefficients for each diffraction order and also full electric and magnetic near field distribution.

Because the grating is usually deposited on the top of a multilayered structure, it can give rise to numerical instabilities related to the substrate modes. To improve numerical stability we employed an enhanced transmittance matrix approach [25]. Despite all these improvements, the RCWA method has some drawbacks. For instance, it can converge very poorly and even diverge for metallic gratings with low losses. On the other hand, the presence of a layer with some losses close to the grating can improve convergence because of the significant damping.

3.4. Theoretical Framework for Parameters Optimization Problem

Figure 4 illustrates the main geometrical features of the structure and gives a depiction of main its geometrical parameters, namely: grating period a , groove depth (etching depth) D , an intermediated metallic layer depth d , and trapezoidal grating profile bases w_1 and w_2 . The last ones

can be expressed through dimensionless parameters such as filling factor $f = w_2/a$, and bases ratio w_1/w_2 .

The optimal value for groove depth was determined from the previous experimental investigation of SPP excitation in aluminum gratings with different modulation patterns [29]. These experiments reveal that the optimal ratio of groove depth to grating period $D/a \approx 0.086$. Therefore the optimal groove depth is $D \approx 0.086 \times 0.63 \mu\text{m} \approx 0.05 \mu\text{m} = 50 \text{ nm}$.

The optimal values for the rest of the geometrical parameters were estimated using numerical simulation. In order to get a better estimate for photoresponse the amount of electromagnetic energy absorbed in each layer was estimated separately. Such an approach allows for separating the parasitic absorption in the metal and the useful absorption in the Si substrate.

Knowing the electromagnetic energy distribution inside each layer we can integrate over the spatial coordinates to find a partial absorption $A_j(\omega)$ inside the j -th layer.

$$A_j(\omega) = \frac{2\pi}{\lambda} \int_0^a \frac{dx}{a} \int_{z_j}^{z_{j+1}} dz \varepsilon''(r, \omega) \frac{|E(r)|^2}{|E_0|^2}, \quad (4)$$

where $\varepsilon''(r, \omega)$ is the local dielectric constant, E_0 is the amplitude of an incident wave, $E(r)$ is the local electric field, $r = (x, y, z)$ is the spatial coordinates.

Figure 5 shows the calculated angular dependencies of the “useful” absorption in the Si substrate for PPPDs with different values of the intermediate layer thickness (d) of the Al grating. A clearly pronounced plasmonic maximum is observed around $\theta_{res} = 15^\circ$, corresponding to SPP excitation. The shape of the resonance curve for such structures is closer to a Fano shape, as shown in the work [21] for gold gratings with a similar groove shape.

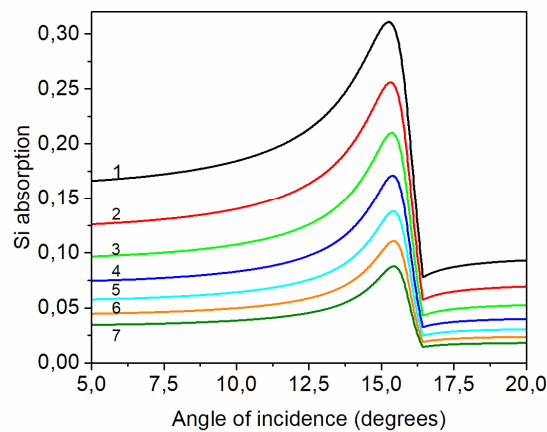


Figure 5. The angle dependences of light absorption in Si substrate for different values of the intermediate layer thickness for the aluminum-based structures. Other parameters: grating period $a=0.63 \mu\text{m}$, etching depth $D=50 \text{ nm}$, filling factor $f=0.5$. Curves 1-7 correspond to thicknesses of 7, 9, 11, 13, 15, 17 and 19 nm, accordingly.

Figure 6a (Curve 1) shows the dependence of the resonant absorption max $A(\theta)$ in the silicon substrate on d for the simulated structure. A monotonic decrease in maximum useful absorption is observed with an increase in the thickness of the intermediate Al layer, in concordance with the decrease of its transparency. However, besides maximizing absorption, another parameter should be optimized to improve sensitivity, namely, the full width at half maximum (FWHM), because narrower absorption peaks correspond to a steeper change of detection signal caused by the resonance frequency shift. Figure 6a (Curve 2) shows the dependence of FWHM on d for the same structure. It is evident that an increase in the thickness of the intermediate Al layer leads to a decrease in FWHM, which is a positive effect. Therefore, it is reasonable to select the goal function in such a way as to take into account FWHM; for example, in this work, we used the ratio of maximal absorption to FWHM: $\max A(\theta)/\text{FWHM}$ (Figure 6b).

The optimal thickness d can be found from an analysis of the goal function $\max A(\theta)/FWHM$.

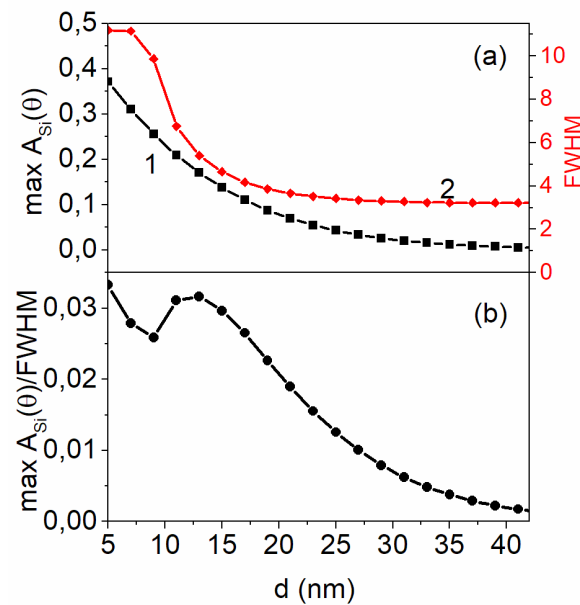


Figure 6. (a) Dependence of the maximum of light absorption in Si ($\max A(\theta)$) (curve 1), and full width at half maximum (FWHM) (curve 2) on the thickness of the intermediate metallic layer, d . (b) Dependence of the goal function $\max A(\theta)/FWHM$ on d .

As seen from Figure 6b, the goal function has two maxima – at a minimum thickness of 5 nm and around 14 nm. Thermally deposited ultra-thin Al films with an effective thickness of 5 nm practically lose their conductivity after oxidation in the air. At the same time, layers with a thickness of 14 nm are well passivated and provide efficient excitation of SPPs. Therefore, for the considered structure, $d = 14$ nm is the optimal thickness of the intermediate Al layer.

The next parameter of the grating that needs to be optimized is the filling factor w_2/a . To choose the optimal value of the filling factor, similar calculations of absorption in the Si substrate were carried out for gratings with different values of w_2/a . Figure 7a shows the dependencies of $\max A(\theta)$ (Curve 1) and FWHM (Curve 2) on the filling factor, which have a non-monotonic character. However, in the dependence of the goal function $\max A(\theta)/FWHM$ on the filling factor (Figure 7b), a clearly pronounced maximum is observed, which allows determining the optimal value of the filling factor for this structure: $w_2/a = 0.36$. Thus, for the considered aluminum grating with an etching depth of 50 nm and a grating period of 0.63 μm , the optimal thickness of the intermediate layer is 14 nm, and the optimal filling factor is 0.36.

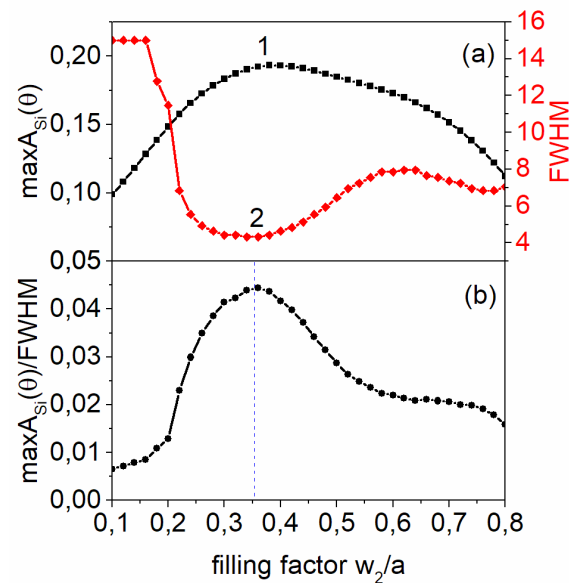


Figure 7. (a) Dependences of the maximum of light absorption in Si ($\max A(\theta)$) (curve 1), and full width at half maximum (FWHM) (curve 2) on the grating filling factor. (b) Dependence of the goal function $\max A(\theta)/FWHM$ on the grating filling factor. The calculations were carried out at the optimal depth of the intermediate Al layer (14 nm).

3. Results and Discussion

Using the obtained results of theoretical modeling, experimental PPPD samples were fabricated with the above-mentioned optimal parameters of the Al grating. The electrophysical properties of the manufactured PPPDs were investigated by the method of current vs voltage characteristics. Figure 8 presents for comparison the current-voltage (I-V) characteristics of the PPPDs with different frontal contacts (gratings): aluminum and gold. The rest of the parameters of both PPPDs, including the characteristics of the gratings, were practically the same. It can be seen that the type of metal has little influence on the current-voltage characteristics of the investigated samples.

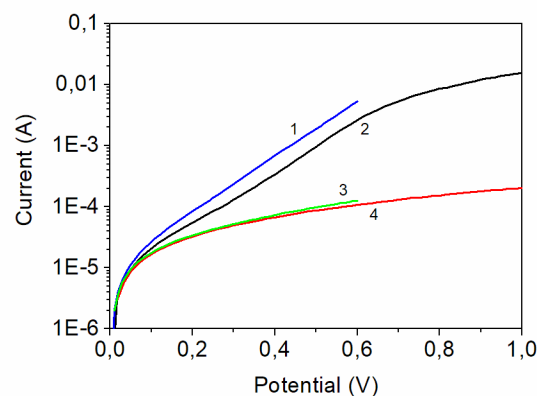


Figure 8. Forward (1,2) and backward (3,4) current–voltage characteristics of the manufactured PPPD with Au (1, 3) and Al (2, 4) frontal plasmon-active contact.

This indicates that the p-n junction in silicon has a crucial effect on the current. The type of plasmon-active metal on the front surface of the PPPD does not affect the I-V characteristics. Both types of PPPDs, with Au and Al frontal plasmon-active contacts have almost the same reverse saturation currents, and the same slope of direct I-V characteristics. The differences may be related to the different areas of contact and the heterogeneity of the properties of the p-n junctions on silicon

used for the production of PPPD. Both types of PPPDs have a non-ideality parameter of the I-V characteristics $n \sim 4$, and a reverse saturation current $I_0 \sim 10^{-5}$ A, which describe their diode properties in the range of 0.1-0.6 V by the general law, without taking into account the series and shunt resistances:

$$I(V) = I_0 \cdot (e^{\frac{qV}{n \cdot k_b T}} - 1), \quad (5)$$

where q is the electron charge, k_b is the Boltzmann constant, T is temperature.

Spectral and angular dependences of photocurrent for fabricated PPPDs are presented in Figures 9a,b and 10a,b, respectively. As observed in Figure 9a, PPPD photocurrent exhibits a pronounced resonance for the case of p-polarized light. This resonance peak shifts towards longer wavelengths with increasing angle of incidence, as predicted by the corresponding Formula (2) of the dispersion dependence for a surface plasmon-polariton wave corresponding to $m = +1$ diffraction order.

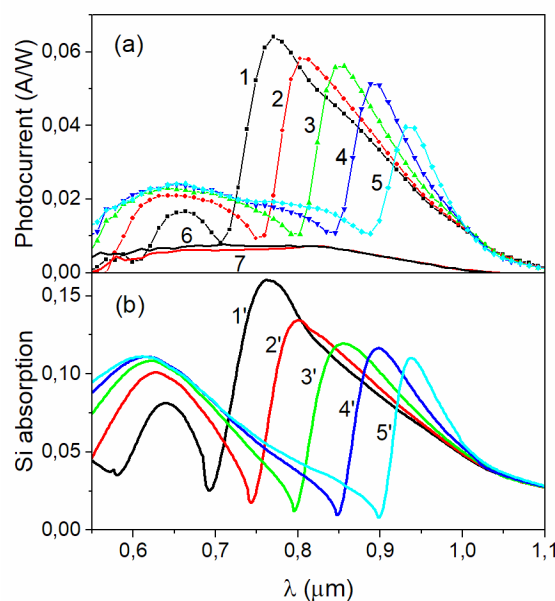


Figure 9. Spectral (a) dependences of the photocurrent of Al-based PPPD in p-polarized light (1-5) and in s-polarized light (6,7), at different angles of incidence: $\theta = 5^\circ$ (1, 6), 10° (2), 15° (3), 20° (4), 25° (5, 7). (b) Numerically simulated Si substrate absorption spectra at the same angles of incidence.

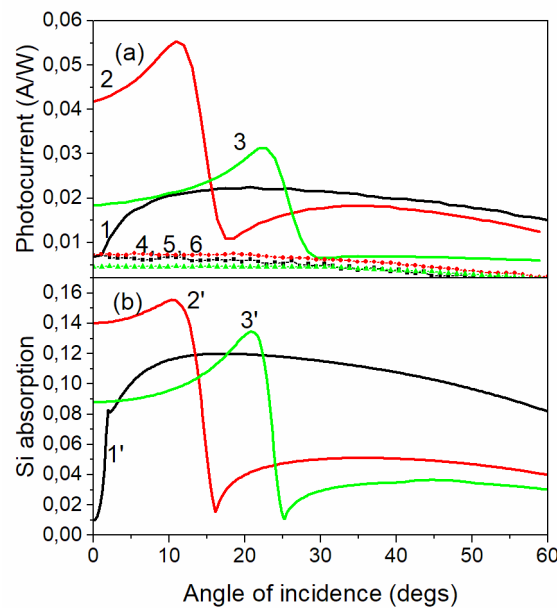


Figure 10. Angular photocurrent dependences for Al-based PPPD in p-polarized light (1-3, 1'-3') and in s-polarized light (4-6), for different wavelengths: 650 nm (1); 808 nm (2); 900 nm (3). (a) experimentally measures data, (b) numerically simulated light absorption by Si substrate.

The polarization sensitivity of PPPD is determined as the ratio of the photocurrent in resonance in p-polarization to the corresponding value when irradiated with light of s-polarization, I_p/I_s . For the investigated PPPDs with optimal parameters of the Al grating, we obtained a value of $I_p/I_s = 8$, the FWHM of the photocurrent spectrum - from 50 to 100 nm, the sensitivity at the resonance maximum $I_{ph} = 0.04-0.06$ A/W. The obtained characteristics of PPPD are comparable to the best results obtained with PPPDs with gold gratings [21]. These practical results open up the prospects of replacing gold in the production of PPPD with aluminum, which significantly lowers their cost.

To verify our theoretical model and analyze the underlying physical mechanisms, we have compared experimental results of photocurrent with the angle and spectral dependences of the light absorption in Si calculated using the RCWA method for trapezoidal profile (Figure 4) with discretization for $N=10$ layers. The calculations were performed for a range of wavelengths and angles of incidence corresponding to the experimental conditions.

Our electrostatics model accounts for all light absorbed within the Si substrate. However, electron-hole pairs generated far from the p-n junction contribute minimally to the photocurrent due to recombination. To address this limitation, we can introduce an effective active layer depth, d_a , into the model. This parameter limits the integration range in Equation (4) to d_a . Since it is difficult to derive a heuristic estimate for d_a , we should treat it as a free parameter when fitting our model to experimental data. The optimal value for d_a thus obtained is $9.2 \mu\text{m}$. The above-mentioned optimal parameters of the Al grating were selected as geometric parameters of the trapezoidal profile.

A direct comparison of the experimental photocurrent spectra (Figure 9a) with the theoretically calculated Si substrate absorption spectra (Figure 9b) reveals a qualitative agreement in the main (1st order) resonance peak positions and their evolution with the angle of incidence. Also, there is a good agreement with respect to the half-width and general shape of peaks: the first-order resonances have almost identical half-width for the experimental and theoretical ones. The tendency to the monotonic decrease of relative peak intensity with the increase of the angle of incidence is also reflected in theoretical calculations. On the other hand, there are some minor discrepancies, namely, in the relative intensity of the second-order (short-wavelength) resonance peaks. It is far more pronounced in the theoretical curves than in the experimental ones. Moreover, the half-width of the second-order resonances is significantly higher. These discrepancies can be related to several factors.

Firstly, the electrodynamic simulation that was conducted gives the power of absorbed light only, so one should be cautious while comparing to the experimentally measured photocurrents. Purely electrodynamic models cannot account for recombination processes, moreover, these processes are spatially dependent, because of doping and surface impact, possible material inhomogeneity. Secondly, the trapezoidal profile model and RCWA layered discretization of the structure profile can also be imperfect approximations. The actual structure profile is much smoother, but such kinds of profiles are much harder to model using RCWA because it requires not only extremely precise profile investigation but also profile discretization with a very small step that leads to a significant increase in computational time.

Similar comparison of measured angular photocurrent dependences data with theoretical simulation of absorption in active Si layer is presented on Figure 10. These curves correspond to three different wavelengths of p-polarized light, therefore there is demonstrated the evolution of SPP resonance maximum with frequency/wavelength shift. The structure of the angular absorption dependency is relatively simple: a single asymmetric SPP related maximum with a dip on the left wing that related to the emergence of the first diffraction order. It is evident from Figure 10 that Si absorption curves repeat the shape of experimental photocurrent dependencies with some small deviation probably related as was mentioned earlier to profile approximation.

The close agreement between the experimental and theoretical results demonstrates the validity of the RCWA method in describing the optical response of PPPDs. However, there may be some discrepancies in peak intensities and half-widths, which may be caused by factors such as manufacturing imperfections, material heterogeneity, or theoretical model limitations such as the use of an approximate trapezoidal profile and neglect of charge carrier recombination processes on surfaces and defects.

4. Conclusions

Using the RCWA method, theoretical simulations of the electromagnetic field intensity distribution in PPPD based on silicon p-n junctions and periodically textured aluminum as the plasmon-carrying metal have been performed. This made it possible to optimize the parameters of the plasmon-carrying grating layer in order to increase the sensitivity of PPPD. Experimental samples of PPPD with aluminum gratings were manufactured and their characteristics were studied. For the PPPDs with optimal grating parameters, we obtained a polarization sensitivity value of $I_p/I_s = 8$, the FWHM of the resonance in photocurrent spectrum ranging from 50 to 100 nm, sensitivity at the resonance maximum $I_{ph} = 0.04-0.06$ A/W, and the angular half-width of the photocurrent resonance $\Delta\theta = 5^\circ$. These characteristics are comparable to the best results achieved with PPPDs using gold gratings. The obtained results pave the way for replacing gold with aluminum in PPPD production, significantly reducing their cost.

Author Contributions: Conceptualization, data curation, S.M., I.I. and Y.L.; methodology, I.I. and S.M.; software, Y.L.; formal analysis, investigation, V.M., V.R., I.M., R.R., M.D., Y.S., V.T., O.Sh., D.K.; writing—original draft preparation, writing—review and editing, S.M., I.I. and Y.L.; project administration, funding acquisition, S.M. All authors have read and agreed to the published version of the manuscript.

Funding: This work was partially supported by National Research Foundation of Ukraine (Grant No. 2022.01/0126, “Development and implementation of a dust-insensitive smoke detector based on a plasmon-polariton photodetector”). S.M. appreciates for funding from the Ministry of Education and Science of Ukraine (Project No. 0122U001956).

Informed Consent Statement: Not applicable.

Data Availability Statement: All data can be provided on reasonable request.

Acknowledgments: The authors acknowledge with thanks MDPI for publication fees waiving of this article. The authors are thankful to P. Lytvyn, A. Korchovyi for AFM analysis, O. Kondratenko for spectroscopic ellipsometry measurements.

Conflicts of Interest: The authors declare no conflicts of interest.

References

1. Gramotnev, D.K.; Bozhevolnyi, S.I. Plasmonics beyond the diffraction limit. *Nature photonics* **2010**, *4*, 83-91.
2. Homola, J. Surface plasmon resonance sensors for detection of chemical and biological species. *Chemical reviews* **2008**, *108*, 462-493.
3. Sipe, J.; Becher, J. Surface-plasmon-assisted photoemission. *JOSA* **1981**, *71*, 1286-1288.
4. Tamm, I.; Dawson, P.; Sellai, A.; Pate, M.; Grey, R.; Hill, G. Analysis of surface plasmon polariton enhancement in photodetection by Al–GaAs Schottky diodes. *Solid-state electronics* **1993**, *36*, 1417-1427.
5. Guo, J.; Wu, Z.; Li, Y.; Zhao, Y. Design of plasmonic photodetector with high absorptance and nano-scale active regions. *Optics Express* **2016**, *24*, 18229-18243.
6. Wu, M.; Xu, N.; Wang, E.; Gen, S.; Zhu, H.; Liu, C.; Cao, J. Nanogratings fabricated by wet etching assisted femtosecond laser modification of silicon for surface plasmon resonance sensing. *Applied Surface Science* **2022**, *603*, 154446.
7. Mamykin, S.; Gnilitskiy, I.; Dusheyko, M.; DeVol, T.; Bliznyuk, V. Femtosecond laser nano-structuring for surface plasmon resonance-based detection of uranium. *Applied Surface Science* **2022**, *576*, 151831.
8. Gnilitskiy, I.; Mamykin, S.V.; Lanara, C.; Hevko, I.; Dusheyko, M.; Bellucci, S.; Stratakis, E. Laser nanostructuring for diffraction grating based surface plasmon-resonance sensors. *Nanomaterials* **2021**, *11*, 591.
9. Brueck, S.; Diadiuk, V.; Jones, T.; Lenth, W. Enhanced quantum efficiency internal photoemission detectors by grating coupling to surface plasma waves. *Applied Physics Letters* **1985**, *46*, 915-917.
10. Gosciniak, J.; Atar, F.B.; Corbett, B.; Rasras, M. Plasmonic Schottky photodetector with metal stripe embedded into semiconductor and with a CMOS-compatible titanium nitride. *Scientific reports* **2019**, *9*, 6048.
11. Sharma, A.K.; Pandey, A.K. Au grating on SiC substrate: simulation of high performance plasmonic Schottky barrier photodetector in visible and NIR regions. *Journal of Physics D: Applied Physics* **2020**, *53*, 175103.
12. Saito, Y.; Yamamoto, Y.; Kan, T.; Tsukagoshi, T.; Noda, K.; Shimoyama, I. Electrical detection SPR sensor with grating coupled backside illumination. *Optics Express* **2019**, *27*, 17763-17770.
13. Glass, A.; Liao, P.; Johnson, A.; Humphrey, L.; Lemons, R.; Olson, D.; Stern, M. Periodically structured amorphous silicon detectors with improved picosecond responsivity. *Applied Physics Letters* **1984**, *44*, 77-79.
14. Berthold, K.; Beinstingl, W.; Berger, R.; Gornik, E. Surface plasmon enhanced quantum efficiency of metal-insulator-semiconductor junctions in the visible. *Applied Physics Letters* **1986**, *48*, 526-528.
15. Brongersma, M.L. Plasmonic photodetectors, photovoltaics, and hot-electron devices. *Proceedings of the IEEE* **2016**, *104*, 2349-2361.
16. Berini, P. Surface plasmon photodetectors and their applications. *Laser & Photonics Reviews* **2014**, *8*, 197-220.
17. Huang, J.A.; Luo, L.B. Low-dimensional plasmonic photodetectors: recent progress and future opportunities. *Advanced Optical Materials* **2018**, *6*, 1701282.
18. Jestl, M.; Köck, A.; Beinstingl, W.; Gornik, E. Polarization-and wavelength-selective photodetectors. *JOSA A* **1988**, *5*, 1581-1584.
19. Dmitruk, N.; Mayeva, O.; Mamykin, S.; Yastrubchak, O.; Klopffleisch, M. Characterization and application of multilayer diffraction gratings as optochemical sensors. *Sensors and Actuators A: Physical* **2001**, *88*, 52-57.
20. Dmitruk, N.; Borkovskaya, O.Y.; Mayeva, O.; Fursenko, O. Polarization-sensitive photocurrents of metal-semiconductor structures with flat and microrelief interfaces. *Microelectronics journal* **1996**, *27*, 37-42.
21. Korovin, A.V.; Dmitruk, N.L.; Mamykin, S.V.; Myn'ko, V.I.; Sosnova, M.V. Enhanced dielectric environment sensitivity of surface plasmon-polariton in the surface-barrier heterostructures based on corrugated thin metal films with quasi-anticorrelated interfaces. *Nanoscale Research Letters* **2017**, *12*, 1-7.
22. Gnilitskiy, I.; Mamykin, S.; Dusheyko, M.; Borodinova, T.; Maksimchuk, N.; Orazi, L. Diffraction Gratings Prepared by HR-LIPSS for New Surface Plasmon-Polariton Photodetectors & Sensors. In Proceedings of the Frontiers in Optics, 2016; p. JW4A. 88.
23. Dmitruk, N.; Klopffleisch, M.; Mayeva, O.; Mamykin, S.; Venger, E.; Yastrubchak, O. Multilayer diffraction gratings Al/GaAs as polaritonic photodetectors. *physica status solidi (a)* **2001**, *184*, 165-174.
24. Moharam, M.; Gaylord, T.K. Rigorous coupled-wave analysis of planar-grating diffraction. *JOSA* **1981**, *71*, 811-818.
25. Moharam, M.; Pommet, D.A.; Grann, E.B.; Gaylord, T.K. Stable implementation of the rigorous coupled-wave analysis for surface-relief gratings: enhanced transmittance matrix approach. *JOSA A* **1995**, *12*, 1077-1086.
26. Palik, E.D. *Handbook of optical constants of solids*; Academic press: 1998; Volume 3.
27. Dan'ko, V.; Dmitruk, M.; Indutnyi, I.; Mamykin, S.; Myn'ko, V.; Shepeliavyyi, P.; Lukaniuk, M.; Lytvyn, P. Au gratings fabricated by interference lithography for experimental study of localized and propagating surface plasmons. *Nanoscale Research Letters* **2017**, *12*, 1-6.

28. Lalanne, P.; Morris, G.M. Highly improved convergence of the coupled-wave method for TM polarization. *JOSA A* **1996**, *13*, 779-784.
29. Indutnyi, I.Z.; Mynko, V.I.; Sopinsky, M.V.; Dan'ko, V.A.; Lytvyn, P.M. Investigation of the surface plasmon-polaritons excitation efficiency on aluminum gratings taking into account diffracted radiation. *Optoelectronics and semiconductor techniques* **2021**, 71-82.

Disclaimer/Publisher's Note: The statements, opinions and data contained in all publications are solely those of the individual author(s) and contributor(s) and not of MDPI and/or the editor(s). MDPI and/or the editor(s) disclaim responsibility for any injury to people or property resulting from any ideas, methods, instructions or products referred to in the content.